Available online at www.sciencedirect.com
ScienceDirect
Surface & Coatings Technology 201 (2006) 4278–4283
SURFACE & COATINGS TECHNOLOGY
www.elsevier.com/locate/surfcoat

Determination of tensile properties by instrumented indentation technique: Representative stress and strain approach

Ju-Young Kim *, Kyung-Woo Lee, Jung-Suk Lee, Dongil Kwon

School of Materials Science and Engineering, Seoul National University, San 56-1, Shillim-dong, Gwanak-gu, Seoul 151-744, Republic of Korea

Available online 11 September 2006

Abstract

Tensile properties can be evaluated by defining representative stress and strain with the parameters obtained from instrumented indentation tests using a spherical indenter. The accuracy of this approach depends strongly on how the contact depth is analyzed and how the representative stress and strain are defined. The primary factors influencing the determination of contact depth, pile-up/sink-in and elastic deflection, were quantified by analyzing indentation morphology by finite element simulation; then plastic pile-up/sink-in behavior was formulated in terms of the strain-hardening exponent and the ratio of indentation depth to indenter radius. For the representative strain, the definition by tangent function was determined to be more appropriate for assessing tensile properties based on derived behaviors of the strain-hardening exponent. This approach was experimentally verified by comparing tensile properties of 10 metallic materials from uniaxial tensile tests and instrumented indentation tests.

Keywords: Instrumented indentation; Representative stress and strain; Tensile properties

1. Introduction

The tensile properties of materials, primarily yield strength and tensile strength, are generally considered the most fundamental mechanical properties. However, specimen preparation for uniaxial tensile tests is destructive and difficult, so that these tests cannot be applied to in-service structural materials. A powerful tool to alleviate this problem is the instrumented indentation test (IIT), which gives accurate measurements of the continuous variation of indentation load as a function of indentation depth [1,2]. Since it has a very high potential for extensive in-field use due to its simple and nondestructive specimen preparation [3–7], numerous investigations of IIT have been performed with the objective of extracting tensile properties by analyzing the indentation load–depth curve [8–14].

In the current study, the true stress–strain relationships were determined from the indentation load–depth curve continuously measured by a spherical indenter based on a representative stress and strain approach. It is essential that the contact depth be established precisely since the representative stress and strain values rely strongly on accurate determination of contact depth. Pile-up/sink-in and elastic deflection, the primary factors influencing the determination of contact depth, were quantified by analyzing indentation morphologies obtained from finite element (FE) simulations. The equation to determine contact depth for a spherical indentation was developed in terms of the strain-hardening exponent and the ratio of indentation depth to indenter radius. The definition of representative strain is in dispute, while the definition of representative stress is not [17,23]. Of the two definitions using sine and tangent functions, the suitability in evaluating tensile properties was analyzed based on derived behaviors of the strain-hardening exponent. Through the determination of precise contact depth and optimum representative stress and strain, tensile properties obtained from tensile tests and IIT were compared for 10 metallic materials.

2. Contact depth equation during spherical indentation

The plastic pile-up/sink-in parameter, h^*_{pile}/h^*_c where h^*_{pile} is the height of plastic pile-up and h^*_c is the elastic contact depth, has an almost linear relation with the strain-hardening exponent at fixed ratio of indentation depth to indenter radius, as shown in Fig. 1 [15]. For different h_{max}/R, where h_{max} is the maximum indentation depth and R is the indenter radius, the plastic pile-up/sink-in parameter has the quadratic relation with h_{max}/R

* Corresponding author. Tel.: +82 2 880 8404; fax: +82 2 886 4847.
E-mail address: juyoung1@snu.ac.kr (J.-Y. Kim).

0257-8972/$ - see front matter © 2006 Elsevier B.V. All rights reserved.
doi:10.1016/j.surfcoat.2006.08.054

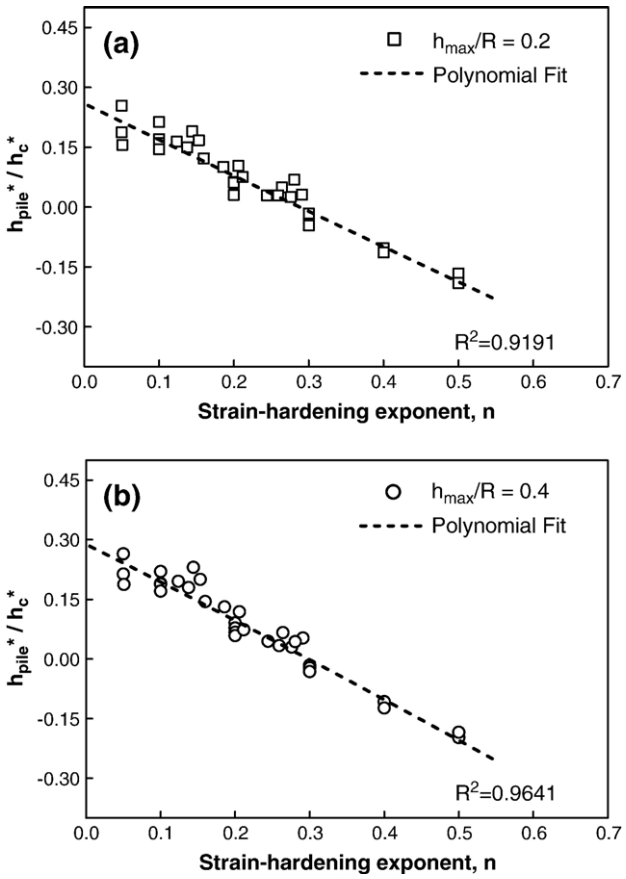

Fig. 1. First step of functionization: polynomial fitting for fixed h_{max}/R [15].

shown in Fig. 2. To reflect the dependence of the plastic pile-up/sink-in parameter on both n and h_{max}/R, a second-order bivariate dependency is introduced as

$$\frac{h^*_{pile}}{h^*_c} = a\left(1 + b_1 n + b_2 n^2\right)\left(1 + c_1 \frac{h_{max}}{R} + c_2 \left(\frac{h_{max}}{R}\right)^2\right), \quad (1)$$

where a, b_1, b_2, c_1 and c_2 are constants. The function describing the plastic pile-up/sink-in effect is determined in two steps: a strain-hardening exponent term is formulated as Eq. (2) for fixed h_{max}/R values, and a variable α is represented as a function of h_{max}/R:

$$\frac{h^*_{pile}}{h^*_c} = \alpha(1 + b_1 n + b_2 n^2), \quad (2)$$

where

$$\alpha = a\left(1 + c_1 \frac{h_{max}}{R} + c_2 \left(\frac{h_{max}}{R}\right)^2\right). \quad (3)$$

In the first step, fitting results are shown in Fig. 1 as procedures to determine a function of n. Even though the term for n was initially taken as a second-order, the fitting results were nearly linear for n. The constants determined from fitting show

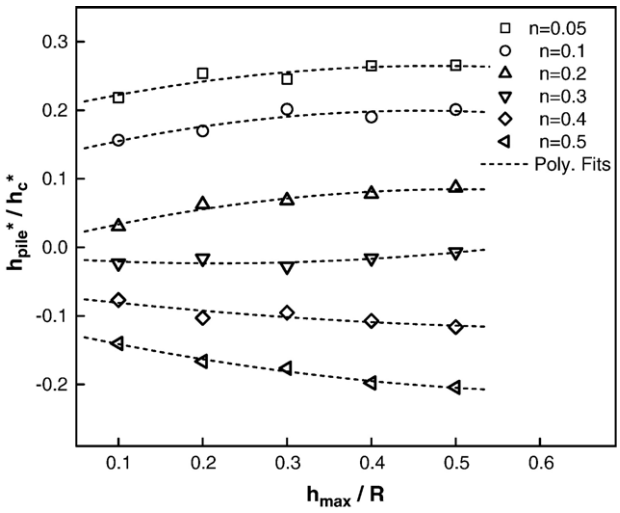

Fig. 2. Plastic pile-up/sink-in parameter as function of h_{max}/R [15].

that the term for the strain-hardening exponent is nearly first-order linear due to the very small constant b_2. The b_1 and b_2 values for different α values, i.e. different h_{max}/R values, are nearly constant, showing the independency between the two terms and the validity of the function shape. The variable α changes with h_{max}/R as shown in Fig. 3, and can be fitted as a second-order term for h_{max}/R. The function for plastic pile-up/sink-in can be expressed by a second-order bivariate:

$$\frac{h^*_{pile}}{h^*_c} = 0.131(1 - 3.423n + 0.079n^2) \times \left(1 + 6.258\frac{h_{max}}{R} - 8.072\left(\frac{h_{max}}{R}\right)^2\right). \quad (4)$$

To show the validity of Eq. (4), Fig. 4 compares the results of the plastic pile-up/sink-in parameter h^*_{pile}/h^*_c from the equation with those from indentation morphology in FE simulation. Agreement is good for materials having different strain-hardening exponents and indentation depth-indenter radius ratio.

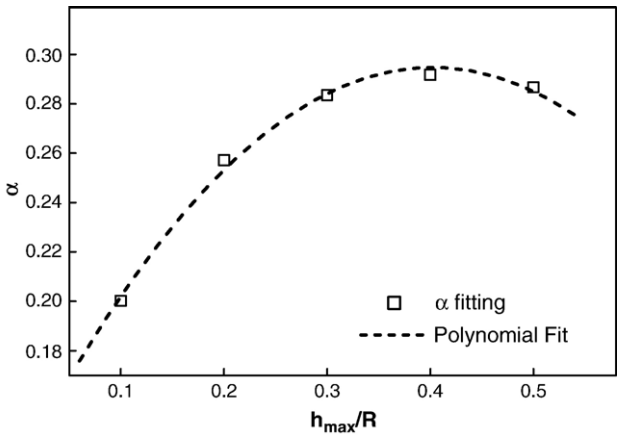

Fig. 3. Determination of α as function of h_{max}/R [15].

3. Representative stress and strain

3.1. Definition of representative stress

The materials experience three deformation stages during spherical indentation [16]: in the elastic stage, deformation can be fully recovered if the load is removed; in the elastoplastic stage, plastic deformation occurs under the indenter; finally, in the fully plastic stage, the plastic deformation zone expands to the surface of the material. Since the IIT is usually performed over several hundreds of N for indentation load and hundreds of micrometer for indenter radius, the elastic and elastoplastic stages are very difficult to detect. Therefore, in the IIT only the fully plastic stage is considered in calculating the true stress [8].

It is well known that the relationship of true stress (σ) and mean pressure (P_m) can be expressed as [17]:

$$\sigma = \left(\frac{1}{\Psi}\right)P_m = \left(\frac{1}{\Psi}\right)\left(\frac{P}{\pi a_c^2}\right), \tag{5}$$

where Ψ is a plastic constraint factor, P is the load, and a_c is the contact radius. Most research on the indentation flow curve has used this definition of true stress. However, the plastic constraint factor has been regarded as a material-independent constant [17] or as a function of the strain-hardening exponent [18,19]. In this study, a constant value of 3.0 was used for the plastic constraint factor, as verified by finite element analysis (FEA) of various materials [13], for which 38 materials, including 14 real materials and 24 ideal materials, were simulated. All materials followed power-law hardening behavior and have yield strength ranging from 200 to 800 MPa, elastic modulus of 100 to 400 GPa, and work-hardening exponent of 0.05 to 0.5; this range covers most metallic materials.

3.2. Definition of representative strain

Definitions of true strain are of two kinds, as suggested by Tabor [17] and Ahn and Kwon [8]. After observing residual indentations made by a spherical indenter on various metals,

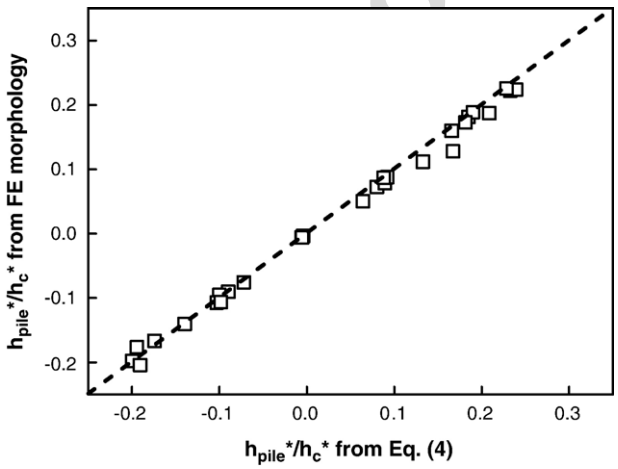

Fig. 4. Comparison of the results for h^*_{pile}/h^*_c from the present function and finite element morphology [15].

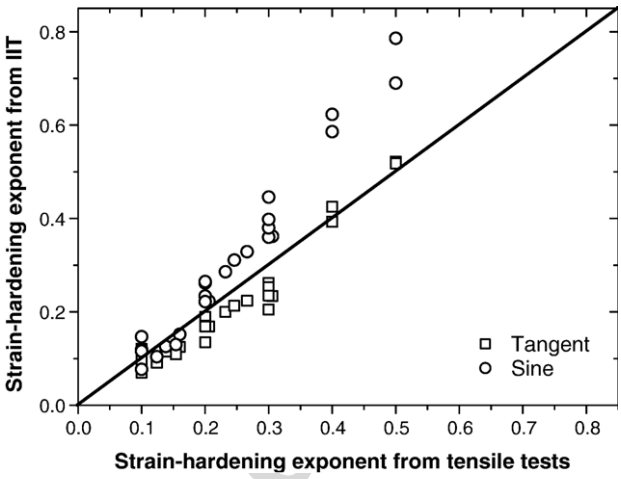

Fig. 5. Strain-hardening exponents measured by experimental instrumented indentation tests and uniaxial tensile tests when analyzed by sine and tangent functions [14].

Tabor proposed an experimental definition of true strain using the sine function:

$$\varepsilon = K_1\left(\frac{a_c}{R}\right) = K_1 \sin\gamma, \tag{6}$$

where K_1 is generally taken as 0.2, R is the indenter radius, and γ is the half-angle between the indenter and the material; this definition has been widely used in similar work. However, the maximum strain should be constrained to be under K_1 (generally 0.2) due to the limitation of the sine function, and this makes it difficult to evaluate the indentation flow curves of ductile metals. On the basis of the deformation shape and strain distribution under a spherical indenter, Ahn and Kwon proposed a new definition using the tangent function. The displacement along the depth axis under the indenter, u_z, can be expressed geometrically as:

$$u_z = h - \left(R - \sqrt{R^2 - r^2}\right), \tag{7}$$

where R is the indenter radius and r is a radius at any point on the depth axis. The shear strain is derived by differentiating the displacement in the depth direction. The maximum shear strain is obtained at $r = a_c$ and Ahn and Kwon obtained the true strain by using a strain proportional constant:

$$\varepsilon = \left(\frac{\alpha}{\sqrt{1-(a_c/R)^2}}\right)\left(\frac{a_c}{R}\right) = \alpha \tan\gamma, \tag{8}$$

where α was determined as 0.14 independent of material properties by FEA for various materials [13]. This definition covers a large range of true strain. Although it also contains the contradiction that maximum strain is infinite when $a_c = R$, the experiment is generally finished by the time a_c reaches 0.6 R. A friction coefficient of 0.2 was used in the computations to model the behavior of the indenter/materials interface; this was determined as the condition best reflecting the actual indentation load–depth curve by comparing the simulation results with that of the continuous indentation test. The influences of friction were examined using friction coefficients of 0.1, 0.2, 0.3, 0.4, and 0.5. The

extracted tensile curves depend on the definition of true strain, which should be verified with the parameters not included in the definition.

3.3. Optimum strain definition based on strain-hardening exponent

The strain-hardening exponent indicates hardening during plastic deformation; it is well known to be an important factor in the amount of pile-up/sink-in in spherical indentation [20]. Generally, plastic deformation occurs from the yield strength to the tensile strength in tensile tests. The strain-hardening exponent is defined as the slope of Eq. (9), where logarithms are used for the axes of true stress and true strain in this range [21]:

$$\log\sigma = \log K + n\ \log\varepsilon. \tag{9}$$

The same method is used in indentation tests when true stress is obtained from Eq. (5) and true strain from Eqs. (6) or (8). If $k\Psi$ is used in Eq. (5) instead of Ψ (k can be any positive number), Eq. (9) becomes:

$$\log\sigma = (\log k + \log\Psi) + n\ \log\varepsilon. \tag{10}$$

This equation indicates that the linear curve shifts parallel to the stress axis and the slope does not vary, which means that the strain-hardening exponent is constant regardless of the plastic constraint factor. A similar concept can be used for α and K_1 in Eqs. (6) and (8). The constants shift the linear curve parallel to the true strain axis, so that the strain-hardening exponent is unchanged. Since this exponent depends only on the functions in the true strain definitions, not on the constants in these definitions, it can be used to determine the appropriate function for the true strain definition.

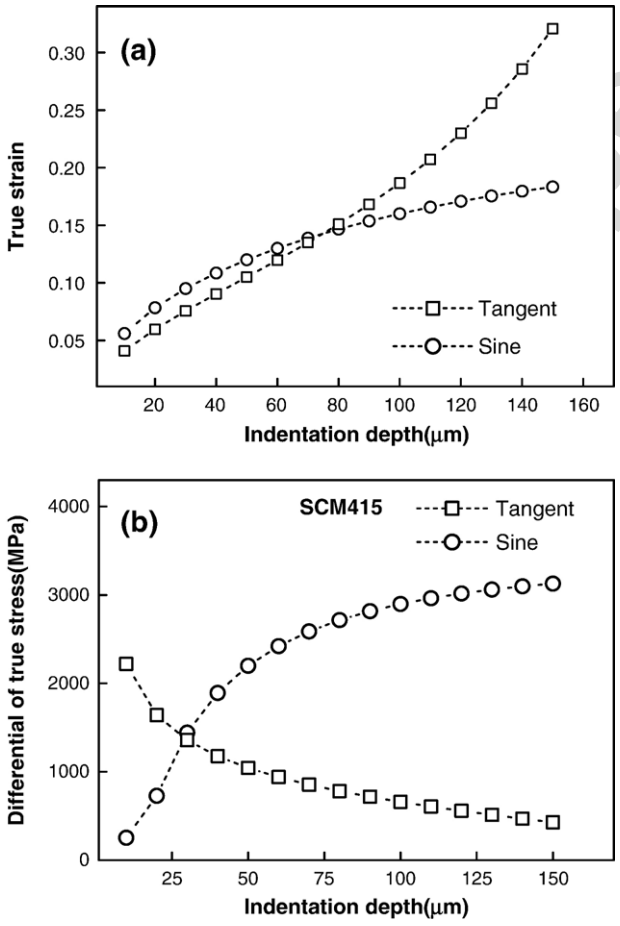

Fig. 6. (a) True strain and (b) differential value of true stress for tangent and sine functions [14].

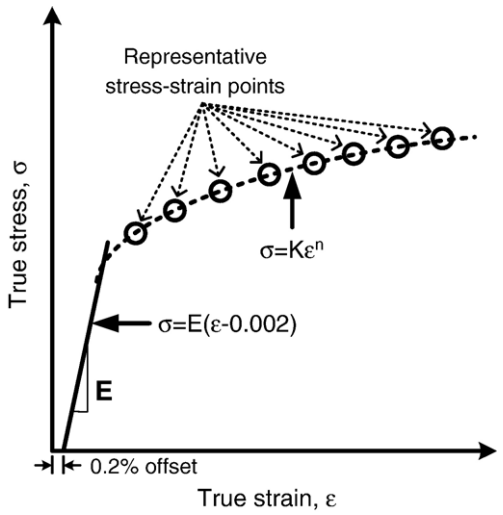

Fig. 7. Schematic: determining tensile properties by representative stress and strain approach.

Fig. 5 shows the strain-hardening exponents derived from each strain definition. The two definitions have similar accuracy below values of 0.2 for the strain-hardening exponent. However, the sine function significantly overestimates above 0.2, while the tangent function produces accurate values. Only the tangent function describes the strain-hardening exponent accurately over a large range.

This difference can be explained by the behavior of the two functions. In general, they have similar values at low angles, and indeed are often taken as identical there. However, the sine function increases slowly to 1 at high angles, while the tangent function goes rapidly to infinity. Fig. 6 presents the true strains calculated by Eqs. (6) and (8) when the indenter radius, α and K_1 are 250 μm, 0.14 and 0.2, respectively. Generally, the flow curves of materials that obey a Hollomon equation ($\sigma = K\varepsilon^n$) show a slow

Table 1
Tensile properties obtained from tensile tests and instrumented indentation tests

Materials	Yield strength (MPa)			Tensile strength (MPa)		
	Tensile	IIT	Error (%)	Tensile	IIT	Error (%)
P91	569.7	558.7	−1.9	772.0	807.5	4.6
S45C	372.9	336.4	−9.8	883.2	843.7	−4.5
SCM21	290.2	314.9	8.5	626.5	609.3	−2.8
SCM415	237.4	230.1	−3.1	616.3	620.7	0.7
SUJ2	306.8	270.2	−11.9	907.7	862.2	−5.0
SKD11	243.4	270.1	11.0	923.1	880.1	−4.7
SKD61	348.9	361.8	3.7	896.5	882.2	−1.6
SKS3	366.4	330.9	−9.7	781.5	810.6	3.7
API X65	451.8	522.9	15.7	610.8	630.3	3.2
API X70	592.9	550.9	−7.1	782.2	770.9	−1.4

increase in true stress in the high-strain range. The sine function shows a slow increase in true strain at large depths, which means high angle and high true strain. Since the increase in true stress is the same for the two definitions, a much greater increase in true stress is observed in the sine function than the tangent function at large depths, as seen in Fig. 6. The differential value of the true stress, $d\sigma/dh$, has a similar physical meaning to the strain-hardening exponent. The sine function has much larger differential values than the tangent function, and this induces overestimates in the strain-hardening exponent. Therefore, the tangent function is the optimum definition for deriving the indentation flow curve of power-law strain-hardening materials.

4. Determination of tensile properties

Fig. 7 shows a schematic of the procedure to determine tensile properties, i.e. yield strength and tensile strength. True stress and strain points are obtained by continuous IIT as explained above. These points are fitted by a constitutive equation (Hollomon equation, $\sigma = K\varepsilon^n$), and K and n are determined. Since the elastic modulus is obtained by IIT, yield strength can be measured from the intersection point between the flow curve and a line with a slope of the elastic modulus 0.2% offset from origin. The ultimate tensile strain should be the same as the strain-hardening exponent by the theory of instability in tension [22], and from this the tensile strength can be determined.

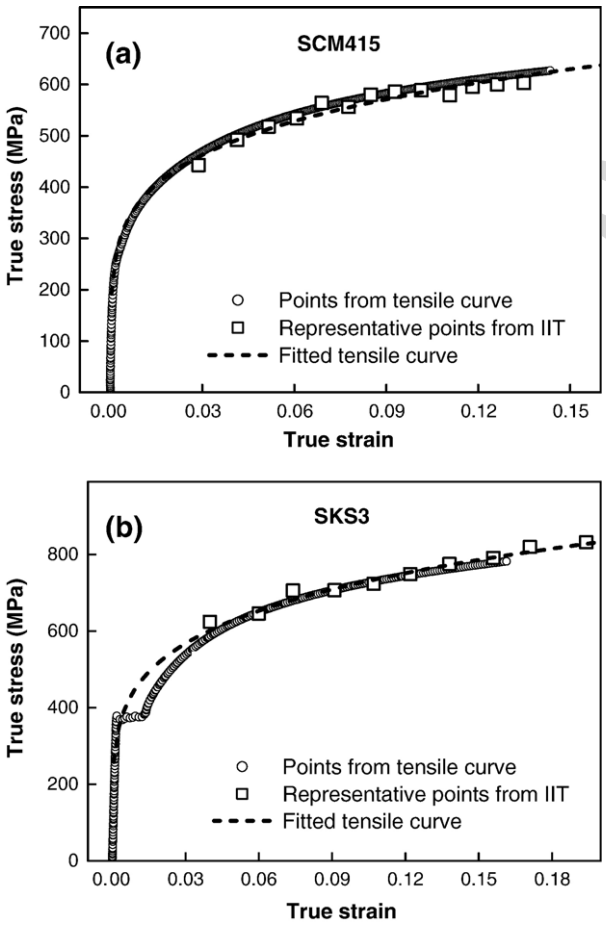

Fig. 8. Comparison between tensile curves from tensile tests and instrumented indentation tests for (a) SCM415 (without Lüders strain) and (b) SKS3 (with Lüders strain).

5. Experimental verification

Ten metallic materials were prepared and their surfaces were finally polished with 1 μm alumina powder. IITs were performed using AIS 3000 equipment made by Frontics Inc. with load resolution 54.88 mN and depth resolution 0.1 μm. The indenter was a WC ball of radius 250 μm, and the loading-unloading speed was 0.1 mm/min. The final maximum indentation was 150 μm and 15 partial unloadings down to 50% of maximum load at each point were performed. To verify our analysis, the true stress and strain curves were measured by tensile tests at cross-head speed of 1 mm/min for specimens with gauge length 25 mm and diameter 6 mm.

The tensile properties obtained from tensile tests and IITs are summarized in Table 1. The error range in tensile strength obtained by IIT was within ±5% of that from tensile tests. For yield strength, the error range was within ±10% except for some materials with high error value (>±10%). The first true stress–strain points were obtained with indentation depth 10 μm, which is about 4% representative strain if contact depth is calculated ignoring elastic deflection and pile-up/sink-in. Yielding happens at strains less than 0.5% for most metallic materials. The true stress–strain points with low strain value affect fitting of the constitutive equation more than the points with high-strain value since the Hollomon equation is a type of exponent function, which induces large deviation in yield strength relative to tensile strength. A possible reason for the high error in yield strength is the presence of Lüders strain [22], as shown in Fig. 8(b). If the length of Lüders strain is defined as ε_L, yield strain ε_y can be estimated as

$$K\varepsilon_y^n = E(\varepsilon_y - 0.002 - \varepsilon_L). \quad (11)$$

For IIT, however, it is difficult to recognize and measure Lüders strain, and we leave this issue for a future study.

6. Conclusions

Tensile properties of 10 metallic materials were obtained using IIT by applying the representative stress and strain approach. Pile-up/sink-in effects during spherical indentation were taken into account by using a function of the strain-hardening exponent and the ratio of indentation depth to indenter radius obtained by FEA. The optimum definition of representative strain was analyzed in terms of the strain-hardening exponent, and the IIT provided more accurate tensile properties when a tangent function is used in the true strain definition. Comparison of tensile properties from IITs with those from uniaxial tensile tests yielded an error range in the tensile strength within ±5%. For yield strength, the error range was within ±10% except for some materials with high error value (>±10%). The larger error range is basically due to the mathematical form of Hollomon equation, and the presence of Lüders strain may have affected the yield strength.

References

[1] M.F. Doerner, W.D. Nix, J. Mater. Res. 1 (1986) 601.
[2] W.C. Oliver, G.M. Pharr, J. Mater. Res. 7 (1992) 1564.
[3] Y.-H. Lee, D. Kwon, Acta Mater. 52 (2004) 1555.
[4] J.-S. Lee, J.-i. Jang, B.-W. Lee, Y. Choi, S.G. Lee, D. Kwon, Acta Mater. 54 (2006) 1101.
[5] J.-Y. Kim, B.-W. Lee, D.T. Read, D. Kwon, Scr. Mater. 52 (2005) 353.
[6] J.-i. Jang, Y. Choi, Y.-H. Lee, D. Kwon, Mater. Sci. Eng., A Struct. Mater.: Prop. Microstruct. Process. 395 (2005) 295.
[7] Y.-H. Lee, K. Takashima, Y. Higo, D. Kwon, Scr. Mater. 51 (2004) 887.
[8] J.-H. Ahn, D. Kwon, J. Mater. Res. 16 (2001) 3170.
[9] J.A. Knapp, D.M. Follstaedt, S.M. Myers, J.C. Barbour, T.A. Friedmann, J.W. Ager III, O.R. Monteiro, I.G. Brown, Surf. Coat. Technol. 103–104 (1998) 268.
[10] A.E. Giannakopoulos, S. Suresh, Scr. Mater. 40 (1999) 1191.
[11] S. Jayaraman, G.T. Hahn, W.C. Oliver, C.A. Rubin, P.C. Bastias, Int. J. Solids Struct. 35 (1998) 365.
[12] K.-D. Bouzakis, N. Michailidis, Thin Solid Films 469–470 (2004) 227.
[13] E.-c. Jeon, M.-K. Baik, S.-H. Kim, B.-W. Lee, D. Kwon, Key Eng. Mater. 297–300 (2005) 2152.
[14] E.-c. Jeon, J.-Y. Kim, M.-K. Baik, S.-H. Kim, J.-S. Park, D. Kwon, Mater. Sci. Eng., A. 419 (2006) 196.
[15] S.-H. Kim, B.-W. Lee, Y. Choi, D. Kwon, Mater. Sci. Eng., A Struct. Mater.: Prop. Microstruct. Process. 415 (2006) 59.
[16] H.A Francis, J. Eng. Mater. Technol. 98 (1976) 272.
[17] D. Tabor, Hardness of Metals, Clarendon Press, 1951.
[18] B. Taljat, T. Zacharia, F. Kosel, Int. J. Solids Struct. 35 (1998) 4411.
[19] J.R. Matthews, Acta Metall. 28 (1980) 311.
[20] Y.T. Cheng, C.M. Cheng, Philos. Mag. Lett. 78 (1998) 115.
[21] ASTM E646, Standard test method for tensile strain-hardening exponents (n-values) of metallic sheet materials, ASTM International, 2002.
[22] G.E. Dieter, Mechanical Metallurgy, McGraw Hill, 1986.
[23] R. Hill, B. Storakers, A.B. Zdunek, Proc. R. Soc. Lond., A 423 (1989) 301.